LU-TP 21-20
June 2021

Primordial Gravitational Waves and ultra-light Dark Matter in a complex singlet extended Standard Model

Sara Wildenor

Department of Astronomy and Theoretical Physics, Lund University

Bachelor thesis supervised by Roman Pasechnik,
Co-supervised by Caterina Doglioni,
and António P. Morais

LUND
UNIVERSITY

Abstract

In this thesis, the consequences of extending the internal symmetries of the standard model with a complex singlet scalar field, are investigated in terms of dark matter phenomenology and the possibility of primordial gravitational wave detection utilizing space based laser interferometry. The scalar potential of the model is constructed with a $\mathbb{Z}_2$ symmetry, which allows for the retainment of a linear and a quadratic coupling parameter, as well as a stable dark matter candidate, and an additional non-zero vacuum expectation value for the real component of the scalar field. The gravitational wave power spectrum is then calculated by implementing cosmoTransition packages, which identifies the phase transition profiles, tunneling solutions and minimum of the effective potential. The results are discussed and compared to the sensitivity curves of the proposed gravitational wave facilities LISA, BBO and DECIGO.

Popular abstract

The Universe is a large and mysterious place. So large that it would take light 93 billion years to cross it (comparable with the rather short 8 minute distance to the Sun), and so mysterious that what little we do know about it, only concerns about 4% of the mass of the Universe - the rest is dark and unknown. What follows here, is a plausible scenario, a little story of what might have happened as the Universe was born, and unimaginable forces replaced some kind of Nothingness with some other kind of Something. It takes place in the aftermath of the Big Bang, during the so called inflation period, where the dynamics of the early Cosmos could provide crucial insight - not only to the true nature of our world, but also regarding the dark aspects of reality; dark matter and dark energy. Little is known about this era, as this part of history is shielded by an opaque veil of light (known as the cosmic microwave background), which our current methods of observation are unable to penetrate. However, gravitational waves have the peculiar ability to propagate freely through all sorts of seemingly impervious obstacles, and with their detection and deciphering, we would be able to open a new window of physics, and look out into a whole new world - or rather a different time of our present world; into the early epochs of the cosmological evolution.

Once upon a long long time ago (more or less the longest time ago it has ever been), in the first millionth of a millionth of a second of what has become an almost 14 billion year long life, the Universe was a hot, boiling primordial soup of primarily radiation and light, with very few similarities to the world we know today. One may think of this rather chaotic state of the Universe as symmetric with respect to its potential energy, but then something happened which where to break this symmetry. As the rapid expansion of the Universe caused it to cool down, bubbles composed of an asymmetric state started to form, move and burst in this boiling soup, which eventually transformed the potential energy of the entire Cosmos into an asymmetric shape. Rather like a phase transition causing a face transition, the appearance of the Universe, was forever changed. The bursting bubbles and the turbulence caused by the bubble walls moving through the blazing plasma, initiated a process so violent that the fabric of space-time itself was disrupted, resulting in the formation of gravitational waves.

For the entire age of the Universe (minus the millionth of a millionth of a second which took place before the considered event), these primordial waves have propagated through the vastness of cosmos at the speed of light, and will most likely continue to do so forever, since nothing seems to slow them down. Thus, clues to the history of the Universe and reality itself, might not be a remote goal, but lie in the nature of these waves, this omnipresent humming echo of the early world dynamics which is causing the space-time around us to gently vibrate. The great technological advancement in experimental research and gravitational wave detection, means it might not be long before (at least hopefully some of) the unknowns concerning the early Universe are unraveled.

Contents

Acknowledgements

I would like to give special thanks to my supervisor Roman Pasechnik, for all his time and dedication towards this thesis. I am also grateful to my co-supervisors Caterina Doglioni and António P. Morais for their valuable input. I would also like to thank Christian Bierlich for his help regarding technical support.

1 Introduction

In the last couple of decades, through the development of the theoretical framework and technological advancements, our knowledge of the world, its constituents and its history, has increased enormously. Recent additions to the fields of particle physics, such as the experimental verification of the Higgs boson [1] and the top quark mass [2], lead us to assume that our current understanding of the particles that make up our reality and their interactions, is - at least to some extent - correct. While the strong and electroweak interactions are described by quantum field theory (QFT) and the standard model (SM), the force of gravity is negligible on the relevant scales in which particles interact, and is therefore separately expressed by the formalism of general relativity. In addition to unifying gravity with the existing framework, there are a number of observed phenomena both in the realm of particle physics and on larger astronomical scales, that the SM are not able to provide an explanation for. One being the presence of Dark Matter (DM), whose existence has been indicated by a number of observables, such as mass displacement in bullet clusters [3], the rotational velocity of spiral galaxies, and the structure of the cosmic microwave background (CMB) [4]. Among other relevant issues that would have to be taken into consideration when developing the physics Beyond the SM, (BSM), are the mass generating mechanism of the neutrino, CP-violation and the baryon asymmetry-problem. Various extensions to the SM have been proposed in order to address some of these problems. Some of the more popular models include Grand Unified Theory (GUT), which features a high temperature merger of the electroweak and strong forces, and supersymmetric (SUSY) models, in which each SM integer (half-integer) spin particle has a half-integer (integer) spin symmetric twin. However successful in providing a solution to baryogenesis, the super-symmetric particles stipulated by SUSY are yet to be detected by colliders, and the absence of experimental verification for any present day BSM theory suggest the need to further develop the framework of the BSM in addition to evolving the experimental framework. The main objective of this thesis is to investigate the implications of a specific BSM scenario, where the symmetries of the SM are extended with an additional complex scalar field. The presence of this field during the inflation era of the early Universe may have resulted in a number of present day detectable phenomena, where the advancement and development of experimental technology provides hope of a possible detection within the coming decades. The goal of this thesis is to analyze the scalar potential of the considered model and thereby being able to identify the probability of a detection by either proposed or present day GW and DM experimental research facilities. Essential characteristics of the phase transition (PT), such as bubble nucleation dynamics and minimization points of the effective potential of the model will be discussed and implemented through cosmoTransitions packages.

The simplest additions to the SM are extensions in the scalar sector, where previous research include minimal extensions with one real scalar [5], or further expansions such as the Two-Higgs Doublet Model [6, 7, 8, 44, 10] and the addition of one or several complex scalar singlets [11, 12, 13, 14, 15, 16]. The complex scalar singlet extension to the SM will

be the focus of attention in this thesis, as it stipulates the conditions in which primordial gravitational waves (PGWs) may have formed through first order electroweak phase transitions (FOEWPTs), features the possibility of a stable DM candidate and the possibility of baryogenesis.

The one complex scalar extension to the SM Lagrangian, referred to as the $cxSM$, is constructed by extending the internal symmetries of the SM with an additional global U(1) symmetry, which, when both softly and spontaneously broken, yields a cold DM candidate as well as FOEWPTs. The presence of these thermal transitions and their effect on space-time, could provide the conditions necessary to generate the baryon-asymmetry observed in the Universe through baryogenesis [11]. The deviation from thermal equilibrium as a result of the strong FOEWPT, would generate a net baryon number, which together with the violation of baryon number and CP symmetries, postulates the Sakharov conditions required for baryogenesis [17]. Through the spontaneous breaking of the U(1) symmetry and the presence of a vev, the real part of the complex singlet is mixed with the Higgs fields and the imaginary part is turned in to a massless Goldstone boson, whose eigenstate represents the additional degree of freedom of the theory. By further allowing for explicit symmetry breaking, the Goldstone boson acquires mass, and thereby becomes a stable scalar DM candidate. An attractive feature of the $cxSM$ is that the DM of the theory have the possibility of a mass range from a few eV to a few TeV, making it a versatile candidate whose prospects of detection - or exclusion by non-detection - could be possible by present or future DM experiments. This thesis will focus on the DM produced by a freeze-in scenario, whose mass lies in the eV range.

Given the apparent influence that gravity has on DM, these phenomena clearly couple to each other in some aspect, making their respective fields inevitably interlinked. The research possibilities which comes with the relatively new addition of GW detection, does not only yield knowledge about gravity, but serves as a compliment to existing and future particle physics experiments by providing further insight on the nature of DM. While the forefront of particle physics is mainly carried out by colliders like the LHC, the delicate detection of GWs is performed by interferometry technology, where perturbations in space-time are distinguished through phase shifts in finely tuned lasers. Technological advancements and improvement in sensitivity of interferometers like those at the Laser Interferometer Gravitational-Wave Observatory (LIGO), has resulted in the successful direct detection of GW signatures produced by astronomical events such as the merger between black holes and between neutron stars. In addition to facilities dedicated to the study of large scale cosmological events, there are a number of strong theoretical and experimental motivations to further examine the field of GWs. These are proposed to have originated during the inflation period of the early Universe, as the violent interaction between expanding vacuum bubbles and the cosmic medium caused ripples in the fabric of space-time. The relic of these strong first order PTs would be a stochastic background of Primordial Gravitational Waves (PWGs), observable at a low frequency range. The opacity of space-time during the inflation era would not affect the propagation of PGWs; thus, their potential detection would enable us to observe the parts of cosmos currently beyond the visible hori-

zon, and thereby provide crucial information regarding the dynamics of the early stages of the Universe. There are other possible sources of PGWs with origins in the inflation era, such as those produced during gravitational reheating [18] or from cosmic strings [19]. However, this thesis will focus on GWs generated through the process of bubble nucleation and a strong FOEWPT, as a consequence of extending the scalar sector of the SM.

This thesis is structured as follows: in section 2, the concept of phase transitions is briefly introduced, section 3 focuses on GWs in terms of methods of detection and the implementation of cosmoTransitions and in section 4 the effective potential is derived. Section 5 provides an introduction to DM and relevant constraints for the considered model and in section 6 numerical results are presented and discussed, while conclusions are given in section 7.

2 Phase Transitions

Roughly a nano-second after the Big Bang, as the radiation-dominated, hot Universe was cooling down, it underwent a PT. If this were to be a PT of the first order - as is the case in many scalar extensions to the SM - the dense primordial plasma would reach what is referred to as the critical temperature T_c, meaning that the coexisting phases have the same free energy. At this stage, symmetry breaking occurs and the effective potential develops a degenerate minimum and a potential barrier, resulting in an non-zero vacuum expectation value, vev. As the temperature reaches below T_c, the system is trapped in the false vacuum of the symmetric state, requiring the transition to the true vacuum of the broken phase, across the potential barrier either through thermal jumps (in the high temperature limit), or by tunneling (at low temperatures) [6]. Analogous to a pot of boiling water, domains of the new broken phase containing the true vacuum form in the hot dense medium. The balance between the surface tension and the pressure difference of the two phases cause small bubbles to collapse, whereas bubbles of a 'critical size' avoid collapse and instead expand and eventually collide, resulting in a phase conversion of the whole system. Through this process, referred to as bubble nucleation, the Universe transitions from a metastable quasi-equilibrium state into a stable equilibrium state. For a more in-depth discussion of the dynamics of bubble nucleation the reader is referred to Refs. [20, 21, 22, 23, 24, 25]

2.1 Phase Transitions in the SM

In the SM the EWPT takes place at $T_c = 160$ GeV [26], as the electroweak symmetry $\mathrm{SU}(2)_L \times \mathrm{U}(1)_Y$ is spontaneously broken to $\mathrm{U}(1)_{em}$. This is a second order PT, also referred to as a crossover, where the two different phases never coexist. Thus, unlike the case for the first order PT, T_c for a second order PT indicates the temperature where the rate of change from one phase to the other is at a maximum. For this to be a PT of the

first order and a GW generating event, the mass of the Higgs is required to be less than 80 GeV [14], which is far below its observed mass of 125 GeV. Hence, in order for the theoretical models to yield PGW producing mechanisms via strong FOPT's and thereby provide the conditions needed for baryogenesis, scalar extensions to the SM, such as the $cxSM$, are required.

3 Gravitational Waves

3.1 Detection

With the new technology of space based laser interferometers, the vibrational background originating from Earth can be eliminated and thereby the sensitivity of the instruments is significantly improved. One proposed project is the Laser Interferometer Space Antenna (LISA). Set to launch in the 2030's, LISA will consist of a constellation of three spacecrafts orbiting the Earth arranged in an equilateral triangle with sides in the range of 10^6 km. The large scale of the project enables it to search for low frequency PGW signatures in the domain between 0.1 mHz and 100 mHz (compared to LIGO's frequency range of 10-1000 Hz [27]), such as those produced around the scale at which electroweak symmetry breaking takes place (approximately 100 GeV). In addition to hopefully providing insight to PGWs and the dynamics of first order PTs in the early Universe, LISA will have a sensitivity range suitable for detecting more recent astronomical events corresponding to low frequency GWs, such as the orbital motion of massive objects. Another proposed project which aims to benefit from the low background noise of space, is the successor of LISA, the Big Bang Observer (BBO) [28]. BBO would operate on the same principles as LISA, but due to its large scale heliocentric orbit and six link triangular interferometer, it would be considerably more sensitive, approximately in the range 0.1 - 1 Hz. While both LISA and BBO are missions operated by NASA and ESA, the third proposed GW detection experiment of interest for this thesis, is a Japanese space mission: the DECi-hertz Interferometer Gravitational wave Observatory (DECIGO) [29]. DECIGO has a sensitivity range of 0.1 - 10 Hz and is proposed to be placed in a heliocentric orbit. Similar to BBO, DECIGO has the primary goal of finding PGWs produced during inflation through direct detection. The GW spectrum generated by the PT of the $cxSM$ will in this thesis be compared to the sensitivity range of both LISA, BBO and DECIGO. The experimental sensitivity curve for LISA were extracted from Ref. [12], for BBO they were taken from Refs. [46, 47], and for DECIGO from [48].

3.2 Gravitational Wave-parameters

The GW spectrum is deduced from a number of quantities related to the dynamics of the phase transition, i.e., transition temperatures and shape of the effective potential, bubble

wall velocity, duration of the PT, and the efficiency factor κ which denotes the amount of latent heat (the fraction of released thermal energy converted either into kinetic energy of the field, κ_ϕ, or bulk motion of the plasma, κ_v). From these phase transition characteristics one may deduce the parameters α, β and T_n, which signify the transition strength, inverse time duration of the phase transition, and nucleation temperature, respectively. The parameter α is related to the potential energy difference between the two vacua in the phase transition, and the quantity β/H is derived in terms of the bounce solution to the Euclidian action at nucleation temperature. The nucleation temperature T_n can be found using CosmoTransitions packages, which identifies the phase transition profiles in terms of tunneling solutions and minimum of the effective potential. These quantities are then used as inputs in order to determine the stochastic GW power spectrum, $h^2\Omega_{GW}$ and the signal-to-noise ratio (SNR). The SNR compares the GW power spectrum of the proposed model to the sensitivity curve of LISA, BBO and DECIGO, and indicates to what extent the detected signal is clear enough for the observed event to be reconstructed and separated from background noise [30, 31].

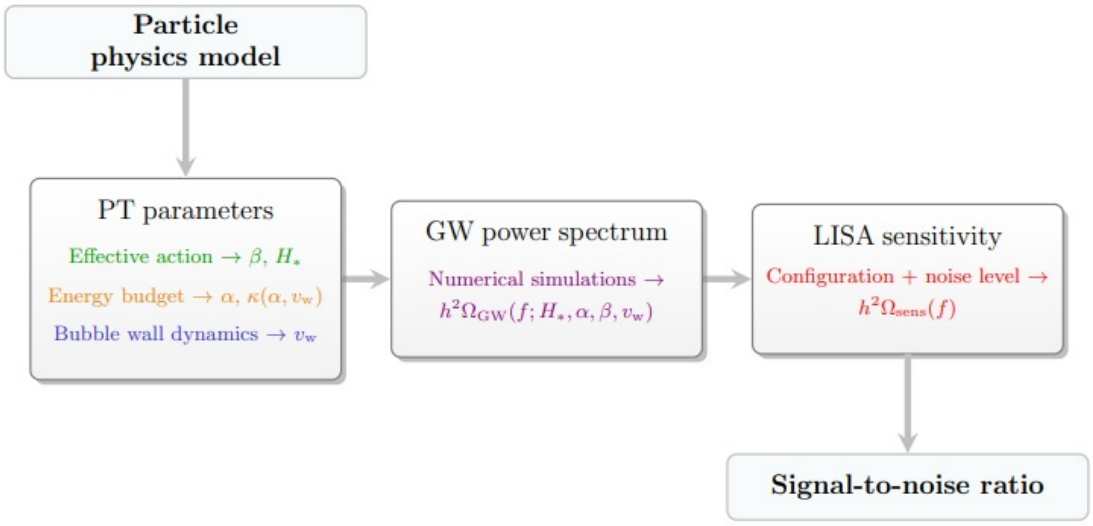

Figure (1) Blueprint for the analysis methods used to identify the GW power spectrum and the SNR for LISA, BBO and DECIGO, based on the dynamics of a PT. Image from Ref. [31].

The power spectrum of the GWs is given in terms of the energy density of the radiation [7];

$$h^2\Omega_{GW} \equiv \frac{h^2}{\rho_c}\frac{\partial \rho_{GW}}{\partial \log f}, \tag{3.1}$$

where ρ_{GW} is the energy density of the GWs, ρ_c is the critical energy density today and f is the frequency. ρ_c is defined as $\rho_c = 3H_0^2/(8\pi G)$, where $H_0 = 100h$ km s^{-1}Mpc^{-1} is the

present day Hubble expansion rate with $h = 0.791 \pm 0.013$, and G is Newton's constant [32]. The disturbance caused by the rapidly expanding bubble walls during the nucleation process give rise to the formation of 'sound shells' of plasma, whose dynamics may be matched to those of sound waves. As have been showed in previous work [33], through the bubble nucleation process the colliding shells generate GWs, which would be detectable as a stochastic background radiation of PGWs in the low frequency range. Collisions between bubble walls and the turbulence in the ionized plasma also contribute to the production of GWs, for which the total energy density of the GW production may be approximated as

$$h^2\Omega_{GW} \simeq h^2\Omega_{sw} + h^2\Omega_{coll} + h^2\Omega_{turb}, \tag{3.2}$$

where $h^2\Omega_{sw}$ is the sound wave contribution, $h^2\Omega_{coll}$ is associated with collisions and $h^2\Omega_{turb}$ is related to the turbulence in the plasma. However, previous Refs. [7, 20, 31] have shown that the main contribution to the GW production derive from the effects of the sound waves and the generated echo which is present even after the PT is completed and thereby enhancing the signal by orders of magnitude. Therefore, I will in this thesis approximate the total energy contribution for the GW production to be of an acoustic origin;

$$h^2\Omega_{GW} \simeq h^2\Omega_{sw}. \tag{3.3}$$

It should be mentioned that there are plausible runaway scenarios, in which the bubble walls reach relativistic velocities and thereby increase the energy contribution from the collisions to a magnitude comparable to that of the sound waves [7, 31]. However, this limit will not be taken into consideration in this thesis, instead bubble wall velocities comparable to the speed of sound in the plasma, c_s, will be of focus for reasons that are discussed in the section below.

3.3 The effective action and nucleation temperature

The energy density of the GWs produced in the FOPT is in general an increasing function of the wall velocity v_b. Thus, a model which yields fast expanding walls is desirable when considering the possibility of PGW detection by facilities like LISA, BBO or DECIGO. However, in order for the PT to accommodate the electroweak baryogenesis, it is required that the bubble wall velocity relative to the surrounding plasma is below the speed of sound [7, 34, 35, 36]. This allows for certain particle species to scatter from the bubble walls where C and CP violation occurs, and diffuse back into the plasma where sphalerons[1] convert the CP asymmetry into a net baryon number. Through the expansion of the bubble walls, the generated net baryon number is shifted into the broken phase of the bubble, where it is preserved due to sufficiently suppressed sphaleron processes. Previous research [23, 37] has shown that there is a viable range for which the wall velocity is sufficient to result

[1]Sphalerons are solutions to field equations, whose trajectory are along the potential over the top of potential barrier, as oppose to the instantaneous solutions which describes tunneling. For more information on this subject see Refs [14, 20].

in detectable GWs, while being slow enough to allow for the process of baryogenesis to take place. This subsonic limit along with faster bubble wall velocities will be taken into consideration when determining the efficiency factor κ, since there is a possibility that the presence of an additional scalar field could have generated substantial PGWs, but no baryogenesis, and vice versa.

In order for the PT to be classified as strong first order, and thereby prevent "washout" [38] of the baryon asymmetry generated in the process, the following requirement has to be satisfied [6, 11];

$$\frac{v_c}{T_c} \gtrsim 1, \tag{3.4}$$

where ν_c denotes the Higgs vev for the SM scenario. 'Deflagrations', i.e., sub-sonic bubble wall velocities, may be denoted as $v_b < v_J = c_s$, where c_s is the speed of sound in the plasma, and v_J is the Chapman-Jouguet speed, which is defined as the speed at which the exit velocity of the fluid in the bubble wall frame is that of the speed of sound [35]. Meanwhile, supersonic wall velocities may be denoted as $v_b > v_J$, and are referred to as detonations. Relevant details regarding the Chapman-Jouguet speed may be found in Appendix B. For the numerical analysis both detonations and deflagration scenarios are examined, but considering that PGWs detectable by either LISA, BBO or DECIGO as a result of deflagrations represent a very fine tuned and rather unlikely scenario [37], the generated data points will in general be derived from detonations with $v_b = 0.95 > v_J$, which maximizes the resulting PGW spectrum.

The bubble wall velocity and the fluid profiles [2] of the plasma depend on the nucleation temperature, T_n, of the EWPT, which signifies the temperature at which the nucleation rate is comparable to the expansion of the Universe. By analysing the Lagrangian and the effective potential of the model of interest, the phase structure of the theory may be calculated for a finite temperature. Given a Lagrangian for a scalar field ϕ, such that

$$\mathcal{L} = \partial_\mu \phi \partial^\mu \phi - V(\phi), \tag{3.5}$$

the nucleation temperature of the PT is found through the three-dimensional bounce solution to the Euclidian action S_3 (see Eq. (3.12)), which reads [6, 20, 34],

$$S_3 = \int d^3x \Big[\frac{1}{2}(\partial_\mu \phi)^2 - V_{eff}(\phi, T)\Big]. \tag{3.6}$$

The bounce solution allows one to describe both high and low temperature scenarios with the same formalism, and it is O(3) symmetric at reasonable high temperatures. Assuming the bubble expansion is spherically symmetric, the action in terms of spherical coordinates is

$$S_3 = 4\pi \int_0^\infty dr\, r^2 \left[\frac{1}{2}\Big(\frac{d\phi}{dr}\Big)^2 + V(\phi, T)\right], \tag{3.7}$$

[2] For more information on this topic the reader is referred to Refs. [23, 39].

where the general equation of motion of the system takes the form

$$V(\phi, T) = \frac{d^2\phi}{dr^2} + \frac{2}{r}\frac{d\phi}{dr}. \tag{3.8}$$

As demonstrated below in the section *Effective potential at a finite termperature*, $V(\phi, T)$ of the Euclidian action is given by the effective potential $V_{eff}(\phi, T) = V_{eff}(h, S, A, T)$, which is found through perturbative expansions to one loop order in 4D.

The nucleation rate of the bubbles at a finite temperature T is given by

$$\Gamma(T) = A(T)e^{-S_3(T)/T}, \tag{3.9}$$

where $A(T)$ is a dynamical prefactor which may generally be estimated on dimensional grounds as $A(T) = \mathcal{O}(T^4)$ [7, 22]. The probability for the PT to exhibit a certain scalar solution to the Euclidian action, may in the high temperature limit be approximated to [6, 20]

$$\Gamma(T) \sim T^4\left(\frac{S_3}{2\pi T}\right)^{3/2} e^{-S_3(T)/T}, \tag{3.10}$$

where T here denotes the nucleation temperature, T_n, which signifies the state where the nucleation rate per unit volume reaches one bubble per Hubble volume per Hubble time [39]:

$$\Gamma(T) \sim H^4. \tag{3.11}$$

By the same methods as have been applied in Refs. [6, 7, 31] one can show that the bubble nucleation temperature for EW-scale transitions may be estimated through

$$\frac{S_3}{T_n} \sim -4\log\left(\frac{T_n}{m_P}\right) \sim 140, \tag{3.12}$$

where m_P is the reduced Planck mass. If the nucleation temperature given in Eq. (3.12) is much smaller than the critical temperature; $T_n << T_c$, the system is said to exhibit supercooling. Meanwhile, if the relation given in Eq. (3.12) has no solution, the PT is a non viable scenario and the system is trapped in the supercooled symmetric phase until the cosmological expansion cause the temperatures to eventually reach zero. Since the relevant processes - baryogenesis and GW production - take place around the nucleation temperature we may modify Eq. (3.4) in order to improve our estimations:

$$\frac{v_n}{T_n} \gtrsim 1, \tag{3.13}$$

where v_n denotes the vev at nucleation temperature. The vevs are not expected to vary significantly with temperature, therefore, Eq. (3.4) and Eq. (3.13) only differ in regards to the critical and nucleation temperature respectively. For the EWPT to classify as strong first order, the value of Eq. (3.4) has been estimated to be in the range of 0.6-1.5, although it should be mentioned that there is no precise consensus on this value. As mentioned

above, the relation $T_n << T_c$ leads to the transition described in Eq. (3.13) being of much stronger nature than the one given by Eq. (3.4), and it has been shown in previous work [6] that a baryogenesis relevant scenario would include transitions where

$$\frac{v_c}{T_c} \gtrsim 0.5. \tag{3.14}$$

For the numerical analysis the relation $\Delta v_n/T_n$ will be implemented. This translates as $\Delta v_n/T_n = (v_n^{final} - v_n^{initial})/T_n$, and signifies the contribution the change of the vev has to the energy budget of the PT.

3.4 The α and β parameters

The inverse duration of the PT $\beta(T)$ is an essential parameter when estimating the GW power spectrum of the theory, and it is defined in terms of the nucleation rate as

$$\beta(T) = \frac{d}{dt} \ln \Gamma(T), \tag{3.15}$$

which enables us to express it relative to the Hubble parameter H for the time of the transition as [7, 23, 39]

$$\frac{\beta}{H} = T_n \frac{d}{dT} \left(\frac{S_3}{T} \right) \Big|_{T=T_n}. \tag{3.16}$$

The GW signals from the relation in Eq. (3.3) are identified through the following generalization [7],

$$\text{signal} \sim \text{amplitude} \times \text{spectral shape}(f/f_{peak}), \tag{3.17}$$

where f is the GW frequency, and f_{peak} is the peak-frequency in terms of the redshift caused by the expansion of the Universe. The relevant peak frequency for the transition we are considering is as follows [7]

$$f_{peak} = 26 \cdot 10^{-6} \left(\frac{1}{HR} \right) \left(\frac{T_n}{100} \right) \left(\frac{g_*}{100 \text{ GeV}} \right)^{\frac{1}{6}} \text{ Hz}, \tag{3.18}$$

where $g_* = 106.75$ is the number of relativistic d.o.f.'s, and the mean bubble separation, R, is given in terms of the dimensionless quantity HR, as

$$HR = \frac{H}{\beta} (8\pi)^{1/3} \max(v_b, c_s), \tag{3.19}$$

with c_S being the speed of sound in the plasma, and v_b the bubble wall velocity. The mean radius between the bubbles is an essential feature of the theory, given that sound shells of size R are predicted to be the dominant source of energy transfer during the phase transition [31]. For a FOPT the bubble sizes are expected to be of a rather large distribution, but approximations in scales of the mean radius and simultaneous bubble

nucleation, has previously in Refs. [35] been successful in providing good results regarding the amplitude and spectral shape of the GW power spectrum.

The strength of the phase transition, α, is usually defined as [7, 35]

$$\alpha = \frac{1}{\rho_\gamma}\left[V_i - V_f - \frac{T}{4}\Big(\frac{\partial V_i}{\partial T} - \frac{\partial V_f}{\partial T}\Big)\right], \tag{3.20}$$

where V_i and V_f are the initial and final potentials of the metastable and stable phases, respectively. The energy density of the radiation at the time of the PT, ρ_γ, in terms of the number of relativistic d.o.f.'s, g_*, is given by [7]

$$\rho_\gamma = g_* \frac{\pi^2}{30} T_n^4. \tag{3.21}$$

The parameter α allows us to define the the fraction of the kinetic energy of the fluid to the total bubble energy, in terms of the efficiency factor κ, as [31]

$$K = \frac{\kappa\alpha}{1+\alpha}. \tag{3.22}$$

Semi-analytical approximations to the relevant efficiency coefficients in terms of κ where taken from Refs. [7, 36], and are given in Appendix B. The acoustic phases in the sound wave formations discussed above, have a lifetime determined by the generation of shocks which take place on a timescale τ_{sh}, and may be denoted relative to the Hubble parameter as a function of R and K [7, 31, 40];

$$H\tau_{sh} = \frac{2}{\sqrt{3}} \frac{HR}{K^{1/2}}. \tag{3.23}$$

This quantity enables us determine the duration of the GW source in units of the Hubble time, resulting in the following relations for the peak energy density [7]:

$$H\tau_{sh} < 1 \longrightarrow h^2\Omega_{GW}^{peak} = 1.159 \cdot 10^{-7} \left(\frac{100}{g_*}\right)\left(\frac{HR}{\sqrt{c_s}}\right)^2 K^{3/2}, \tag{3.24}$$

$$H\tau_{sh} \simeq 1 \longrightarrow h^2\Omega_{GW}^{peak} = 1.159 \cdot 10^{-7} \left(\frac{100}{g_*}\right)\left(\frac{HR}{c_s}\right)^2 K^{2}, \tag{3.25}$$

with the source lasting less or approximately equal to the Hubble time, respectively. The two expressions given in Eqs. (3.24) and (3.25) are valid for both deflagrations and detonations, and the relevant numerical factors where taken from Ref. [31] and may be found in Appendix B. In accordance with the relation in Eq. (3.17) the GW spectrum is found by multiplying the appropriate amplitude in Eq. (3.24) or (3.25) with the spectral function which takes the following form [7]

$$h^2\Omega_{GW} = h^2\Omega_{GW}^{peak} \left(\frac{4}{7}\right)^{-7/2} \left(\frac{f}{f_{peak}}\right)^3 \left[1 + \frac{3}{4}\left(\frac{f}{f_{peak}}\right)\right]^{-7/2}. \tag{3.26}$$

3.5 Signal to noise ratio

In order to determine the viability of the detected GW radiation signatures w.r.t. the background, the proposed GW power spectrum is compared to the sensitivity range of LISA, BBO and DECIGO. As demonstrated above, thermodynamical quantities lead to a possible calculation of $h^2\Omega_{GW}$, which enables one to finally estimate the SNR through the standard formula [31]

$$SNR = \sqrt{\tau_m \int_{f_{min}}^{f_{max}} df \left[\frac{h^2\Omega_{GW}(f)}{h^2\Omega_{sens}(f)}\right]}, \tag{3.27}$$

where $\tau_m =$ is the duration of mission, and $h^2\Omega_{sens}$ is the nominal sensitivity of the considered GW detection experiment, which is formulated in terms of the spectral density $S_h(f)$ as

$$h^2\Omega_{sens}(f) = \frac{2\pi^2}{3H_0^2} f^3 S_h(f). \tag{3.28}$$

$h^2\Omega_{GW}$ is for deflagration scenarios equal to the expression in Eq. (3.24). Given the long observation time of the mission there is a great probability of a future detection of GWs with an acoustic origin - even considering they are distinctively weaker than those produced by supersonic detonation or runaway models.

4 One complex scalar extended model

4.1 Tree Level Potential

The *cxSM* is built by adding a complex scalar singlet field, $\mathbb{S}$, to the SM Lagriangian. $\mathbb{S}$ couples only to the fermions and bosons of the SM through the Higgs, often referred to as the "Higgs portal". Thus, the only interaction terms between $\mathbb{S}$ and the SM is found in the scalar potential $V(H, \mathbb{S})$. In order to simplify this potential we impose two symmetries to the theory:

a) $\mathbb{S} \to -\mathbb{S}$, throughout this thesis referred to as $\mathbb{Z}_2$. This discrete symmetry results in the elimination of all terms in the scalar potential containing odd powers of $\mathbb{S}$. It also enables the stability of the DM particle through symmetry breaking of the last two terms of the potential in Eq. (4.29), and thereby avoiding the issue of cosmological domain walls.

b) By requiring that the *cxSM* scalar potential possess a global U(1) symmetry, all terms containing complex coefficients in the scalar potential may be eliminated.

The resulting scalar potential of the $cxSM$ is then given by

$$\begin{aligned} V_{cxSM}(H,\mathbb{S}) =& \frac{\mu_h^2}{2}H^\dagger H + \frac{\lambda_h}{4}(H^\dagger H)^2 \\ & \frac{\mu_S^2}{2}|\mathbb{S}|^2 + \frac{\lambda_{hS}}{2}H^\dagger H|\mathbb{S}|^2 + \frac{\lambda_S}{4}|\mathbb{S}|^4 \\ & + \Big(|a_1|e^{i\phi_{a1}}\mathbb{S} + \frac{1}{4}|b_1|e^{i\phi_{b1}}\mathbb{S}^2 + c.c.\Big), \end{aligned} \tag{4.29}$$

where H represents the complex Higgs doublet, which is usually parametrized in terms of the physical field; $H = \begin{pmatrix} 0 \\ \frac{h+v}{\sqrt{2}} \end{pmatrix}$, with the Higgs vev $v_h = 246$ GeV, and $\mathbb{S}$ is given by $\mathbb{S} = (S + iA)\sqrt{2}$. The appearance of the potential $V_{cxSm}(H,\mathbb{S})$ is identical to one obtained by the addition of of two real scalar singlets, each corresponding to the imaginary and real components of $\mathbb{S}$.

Before any symmetry breaking occurs, the presence of a singlet vev at zero temperature results in the real component of $\mathbb{S}$, S, appearing as a massive scalar and mixing with the neutral component of the Higgs. The imaginary part, A, is a massless Goldstone boson, which - although stable - is not phenomenologically viable since its presence would modify the effective number of light neutrinos in the Universe [11]. By introducing a soft breaking of the global U(1) symmetry, more specifically to the last two terms of the scalar potential, A requires mass and thereby becomes a viable cold DM (CDM) candidate. Breaking terms, such as the one proportional to b_1, which do not generate additional soft symmetry-breaking terms when normalized [11], are preferred. The symmetry of the potential would have been retained for $a_1 = 0$, but since spontaneously broken symmetries tend to give rise to cosmological domain walls [13], an explicit $\mathbb{Z}_2$-breaking term proportional to a_1 is required.

On the basis of the given scalar potential one can consider a number of different scenarios depending on the choice of vev in relation to the type of symmetry breaking. This have been studied in greater detail in Refs. [11, 13]. However, this thesis will from now on focus on the scenario where both $a_1 \neq 0$ and the singlet acquires a vev, since these requirements must be fulfilled in order for the theory to yield a stable CDM candidate as well as an EWFOPT. In order to further simplify Eq. (4.29), the phase ϕ_{a1} can be eliminated through absorption and redefinition of a_1 and $\mathbb{S}$. In accordance with convention, $\phi_{b1} = \pi$ is chosen [13]. By expanding the scalar potential with $H = h/\sqrt{2}$ and $\mathbb{S} = (S + iA)/\sqrt{2}$, we obtain the tree-level potential:

$$\begin{aligned} V_0(h,S,A) =& \frac{\mu_h^2}{4}h^2 + \frac{\lambda_h}{16}h^4 + \frac{\lambda_{hS}}{8}h^2(S^2+A^2) + \frac{1}{4}(\mu_S^2 - b_1)S^2 \\ & + \frac{1}{4}(\mu_S^2 + b_1)A^2 - \sqrt{2}a_1 S + \frac{\lambda_S}{8}S^2A^2 + \frac{\lambda_S}{16}(S^4 + A^4). \end{aligned} \tag{4.30}$$

4.2 Minimizing the tree-level potential

In order to obtain the mass eigenstates of $\mathbb{S}$, which are generated by fluctuations around the singlet vev, we minimize the potential in Eqn. (4.30) w.r.t. each field. For a full analysis of the scalar potential, the mass eigenstates for both the zero temperature as well as the finite temperature scenario will have to be identified and calculated. The global minimum of the tree-level potential is found through the following minimization conditions:

$$\frac{\partial V_0}{\partial h} = 0, \quad \frac{\partial V_0}{\partial S} = 0, \quad \frac{\partial V_0}{\partial A} = 0. \tag{4.31}$$

For the zero temperature scenario we require that $\langle H \rangle = h/\sqrt{2} = v_h/\sqrt{2}$, with v_h being the Higgs vev, together with the conventional definition $\langle \mathbb{S} \rangle = (v_S + iv_A)$, where v_S and v_A represents the vev of the real and imaginary field components of $\mathbb{S}$. In order to ensure that there are no mixing between the scalar and pseudoscalar mass eigenstates, the vev of the imaginary component of the scalar field has to be zero; i.e., $v_A = 0$. For scenarios where $v_A \neq 0$, the reader is referred to Ref. [11]. Applying the above mentioned conditions we obtain the following equations:

$$\begin{aligned} \frac{\partial V_0}{\partial v_h} &= \frac{v_h}{2}\Big(\mu_h^2 + \frac{\lambda_h v_h^2}{2} + \frac{\lambda_{hS}(v_S^2 + v_A^2)}{2}\Big) = 0 \\ \frac{\partial V_0}{\partial v_S} &= \frac{v_S}{2}\Big(\mu_S^2 - b_1 + \frac{\lambda_{hS} v_h^2}{2} + \frac{\lambda_S(v_S^2 + v_A^2)}{2}\Big) - \sqrt{2}a_1 = 0. \end{aligned} \tag{4.32}$$

This yields the two tadpole conditions

$$\begin{aligned} \mu_h^2 &= -\frac{\lambda_h v_h^2}{2} - \frac{\lambda_{hS} v_S^2}{2}, \\ \mu_S^2 &= b_1 + \frac{2\sqrt{2}a_1}{v_S} - \frac{\lambda_{hS} v_h^2}{2} - \frac{\lambda_S v_S^2}{2}, \end{aligned} \tag{4.33}$$

which ultimately allow us to eliminate the parameters μ_h^2 and μ_S^2, and instead express the zero temperature masses in terms of the Higgs vev v_h, the singlet vev v_S, and the coupling parameters λ_h, λ_S and λ_{hS}.

In order to obtain the finite temperature mass eigenstates we examine the second derivative

of the tree-level potential w.r.t. h, S and A;

$$\begin{aligned}
m_h^2 &= \frac{\partial^2 V_0}{\partial h^2} = \frac{\mu_h^2}{2} + \frac{3\lambda_h h^2}{4} + \frac{\lambda_{hS}(S^2+A^2)}{4}, \\
m_S^2 &= \frac{\partial^2 V_0}{\partial S^2} = \frac{1}{2}(\mu_S^2 - b_1) + \frac{\lambda_{hS} h^2}{4} + \frac{\lambda_S(3S^2+A^2)}{4}, \\
m_A^2 &= \frac{\partial^2 V_0}{\partial A^2} = \frac{1}{2}(\mu_S^2 + b_1) + \frac{\lambda_{hS} h^2}{4} + \frac{\lambda_S(S^2+3A^2)}{4}, \\
m_{hS}^2 &= \frac{\partial^2 V_0}{\partial h \partial S} = \frac{\partial^2 V_0}{\partial S \partial h} = \frac{\lambda_{hS} hS}{2}, \\
m_{hA}^2 &= \frac{\partial^2 V_0}{\partial h \partial A} = \frac{\partial^2 V_0}{\partial A \partial h} = \frac{\lambda_{hS}}{2} hA, \\
m_{SA}^2 &= \frac{\partial^2 V_0}{\partial S \partial A} = \frac{\partial^2 V_0}{\partial A \partial S} = \frac{\lambda_S}{2} SA,
\end{aligned} \tag{4.34}$$

where each expression in Eq. (4.34) can be arranged in a matrix form in the following way

$$M_{cxSM}^2 = \begin{bmatrix} m_h^2 & m_{hS}^2 & m_{hA}^2 \\ m_{hS}^2 & m_S^2 & m_{SA}^2 \\ m_{hA}^2 & m_{SA}^2 & m_A^2 \end{bmatrix}. \tag{4.35}$$

For the numerical analysis the thermal masses for h, S and A are calculated by diagonalizing the M_{cxSM}^2 above in Eq. (4.35). Other field dependent thermal masses are given in Appendix A.

By combining Eqns. (4.34) and (4.33), the eigenvalues for the zero temperature masses may be expressed as

$$\begin{aligned}
m_h^2 &= \frac{1}{2}\lambda_h v_h^2, \\
m_S^2 &= \frac{\lambda_S v_S^2}{2} + \frac{\sqrt{2} a_1}{v_S}, \\
m_A^2 &= b_1 + \frac{\sqrt{2} a_1}{v_S}, \\
m_{hS}^2 &= \frac{\lambda_{hS} v_h v_S}{2}.
\end{aligned} \tag{4.36}$$

As a result of the spontaneously and explicit breaking of the U(1) symmetry, the linear parameter a_1 and the quadratic parameter b_1 will give mass to the Goldstone boson of the $cxSM$. The stability of the DM candidate is provided by the $\mathbb{Z}_2$ symmetry, and therefore the scalar DM of the $cxSM$ is referred to as Z_2xSM. As can be seen in Eq. (4.34), there is no mixing between A and the h and S fields. Meanwhile, the non-zero entry for m_{hS}^2, causes the real component of the singlet to mix with the SM Higgs, resulting in two massive scalars, whose mass eigenstates we denote as h' and S', reflecting their "Higgs-like" and "singlet-like" state respectively. Their masses are given by the eigenvalues of the 2x2 upper

left quadrant of Eq. (4.35), which in full details becomes[3]

$$m^2_{h_{1,2}} = \frac{\lambda_h v_h^2}{4} + \frac{\lambda_S v_S^2}{4} + \frac{\sqrt{2}a_1}{2v_S} \pm \sqrt{\Big(\frac{\lambda_h v_h^2}{4} - \frac{\lambda_S v_S^2}{4} - \frac{\sqrt{2}a_1}{2v_S}\Big)^2 + \frac{\lambda_{hS}^2 v_h^2 v_S^2}{4}}. \tag{4.37}$$

Which one of the eigenstates h' and S' that corresponds to m_{h_1} or m_{h_2}, will depend on ones choice of parameters. The two expressions in Eq. (4.37) may be more generally expressed as

$$\begin{aligned} m^2_{h_{1,2}} &= \frac{1}{2}\Big[m_h^2 + m_S^2 \pm \sqrt{(m_h^2 - m_S^2)^2 + 4(m_{hS}^2)^2}\Big] \\ &= \frac{1}{2}\Big[\mathrm{Tr}(M_{cxSM}) \pm \sqrt{(\mathrm{Tr}(M_{cxSM}))^2 - 4\mathrm{Det}(M_{cxSM})}\Big], \end{aligned} \tag{4.38}$$

with the requirement that $\mathrm{Det}(M_{cxSM}) > 0$ in order to ensure that the masses are real positive numbers [13]. For $v_h^2 > v_S^2$ the heavier eigenstate m_{h_2} will correspond to h', and should the singlet vev have a mass greater than the Higgs vev, then $S' = m_{h_2}$. For the numerical analysis Eq. (4.38) may be recast to the more convenient expression

$$m^2_{h_{1,2}} = \frac{1}{2}\big[m_h^2 + m_S^2 \pm (m_h^2 - m_S^2)\sec 2\theta\big]. \tag{4.39}$$

Given that h' and S' are orthogonal representations of the mass eigenstates, we may express them in terms of their mixing eigenstates such that

$$\begin{bmatrix} h' \\ S' \end{bmatrix} = \begin{bmatrix} \cos\theta & \sin\theta \\ -\sin\theta & \cos\theta \end{bmatrix} \begin{bmatrix} h \\ S \end{bmatrix}, \tag{4.40}$$

which gives us the relations

$$\begin{aligned} h' &= h\cos\theta + S\sin\theta, \\ S' &= S\cos\theta - h\sin\theta. \end{aligned} \tag{4.41}$$

As is evident in Eq. (4.41), the h' and S' coupling to the fermions of the SM via the Higgs, is reduced by a factor $\cos\theta$ and $-\sin\theta$ respectively. Subsequently the mixing angle at tree level is given by [11]

$$\begin{aligned} \tan 2\theta &= \frac{2m_{hS}^2}{m_h^2 - m_S^2} \\ &= \frac{\lambda_{hS} v_h v_S}{\frac{1}{2}\lambda_h v_h^2 - \frac{1}{2}\lambda_S v_S^2 - \frac{\sqrt{2}a_1}{v_S}}. \end{aligned} \tag{4.42}$$

The range $-\pi/4 < \theta < \pi/4$ is chosen for the mixing angle, as to ensure the nature of h' maintains "Higgs-like" and S' "singlet-like" [12, 13, 14]. By assuming the Higgs-like state, h', to have a mass of 125.09 GeV and thereby taking the singlet state to be the heavier scalar, current constraints on the mixing angle requires it to be in the limit of [31]

$$|\sin\theta| \lesssim 0.2 - 0.3, \tag{4.43}$$

depending on the mass of S'. This constraint is a result of direct searches at the LHC and EW precision measurements, and is applicable in the mass range S' ∼125 GeV - 1 TeV [31].

[3]See Refs. [11, 12, 13, 14] for further discussion regarding this and the details throughout this section.

4.3 Vacuum stability

The vacuum stability of the $cxSM$ potential at tree level is ensured by the fulfillment of the following requirements:

$$\begin{aligned} \lambda_h &> 0, \\ \lambda_S &> 0, \\ \lambda_h\lambda_S &> \lambda_{hS}^2. \end{aligned} \tag{4.44}$$

The first two conditions may be derived from Eq. (4.36), and ensure that the potential is bounded from below. The last condition guarantees that the mass-squared eigenvalues of the mix between the real component of the singlet and the Higgs doublet is positive. For more on details on the vacuum stability of the $cxSM$, the reader is referred to Refs. [11, 13, 15, 16].

4.4 Effective potential at a finite temperature

The dynamics of the EWPT (as discussed in section "Phase Transitions") are determined by the shape of the effective potential $V_{eff}(h, S, A, T)$, which describes the energy density of a homogeneous state at a finite temperature T. In order to fully comprehend the dynamics of the phase transition, the temperature dependence of the effective potential is a crucial aspect as it allows one to study the development of the different vacua in the cooling process through perturbation theory.

The scalar potential analysis using cosmoTransition is performed in three parts: by identifying tunneling algorithms and phase tracing algorithms, and the implementation of the model of interest. This is done through the generic potential class, which calculates the one-loop corrections from the field-dependent mass spectrum using the Coleman-Weinberg potential $V_{CW} = (h, S, A, T)$, found below in Eq. (4.46) [22].

The additional degree of freedom of the $cxSM$ that is represented by A, will (due to self interaction) generate a one loop Coleman-Weinberg potential $V_{CW} = (h, S, A, T)$, whose contribution to the effective potential needs to be examined along the tree level potential in Eq. (4.30). In addition to this one must also include thermal corrections, here denoted as $V_{th}(h, S, A, T)$, as well as the counter term $V_{ct}(h, S, A)$. Thus, we may express the effective potential at a finite temperature as

$$V_{eff}(h, S, A, T) = V_0(h, S, A) + V_{CW}(h, S, A, T) + V_{th}(h, S, A, T) + V_{ct}(h, S, A). \tag{4.45}$$

The Coleman-Weinberg potential, calculated in the Landau gauge and renormalized in the $\overline{MS}$ scheme, is given by

$$V_{CW}(h, S, A, T) = \sum_i n_i \frac{m_i^4(h, S, A, T)}{62\pi^2} \Big[ln\Big(\frac{m_i^2(h, S, A, T)}{\mu_R^2}\Big) - c_i \Big], \tag{4.46}$$

where the sum i runs over all scalar, fermion and boson contributions, n_i denotes the number of degrees of freedom for the each respective field, m_i represent the field dependent mass, μ_R is the renormalization scale which we fix to $\mu_R^2 = v_h^2$, and $c_i = 3/2$ for bosons, and $c_i = 1/2$ for fermions [7].

The lowest-order one-loop thermal correction term for a finite temperature T, is obtained as

$$V_{th}(h,S,A,T) = \frac{T^4}{2\pi^2}\left[\sum_b n_b J_B\left(\frac{m_i^2(h,S,A,T)}{T^2}\right) - \sum_f n_f J_F\left(\frac{m_i^2(h,S,A,T)}{T^2}\right)\right] \quad (4.47)$$

where

$$J_{B,F}(a^2) = \int_0^\infty x^2 dx \ln\left[1 \mp \exp(-\sqrt{x^2+a^2})\right]. \quad (4.48)$$

The negative and positive sign in the logarithmic term in Eq. (4.48) corresponds to bosonic and fermionic contributions respectively. J_B and J_F are the thermal integrals for the bosons and fermions, which in the high temperature limit, where $a \equiv m/T << 1$, can be approximated as [6]

$$\begin{aligned} J_B(a^2) &\simeq \frac{-\pi^4}{45} + \frac{\pi^2}{12}a^2 + \frac{\pi}{6}a^3 + \mathcal{O}(a^4), \\ J_F(a^2) &\simeq \frac{7\pi^4}{360} - \frac{\pi^2}{24}a^2 + \mathcal{O}(a^4). \end{aligned} \quad (4.49)$$

Fermionic contributions to the thermal corrections other than that of the top quark are excluded due to the relative smallness of their Yukawa couplings. Thus, the thermal corrections, expanded at order a^2, reduces to [6]

$$V_{th}(h,S,A,T) = \frac{T^2}{24}\left[\mathrm{Tr}(M_{h,S,A}^2) + \sum_{i=W,Z,\gamma} n_i m_i^2 + \sum_{i=f_i} \frac{n_i}{2} m_i^2\right]. \quad (4.50)$$

where fermionic contributions for all three generations are taken into consideration in the last sum with $f_i = t, b\tau, c, s, \mu, u, d, e, \nu_{1,2,3}$, and the coefficient n_i represents the number of d.o.f for each given particle, these are given in Appendix A.

The presence of the T^2 term in the effective potential usually indicates that there is a symmetry restoration and therefore a collapse of perturbation theory at $T \sim T_c$. This requires an all-order resummation of higher order corrections, which is accomplished by replacing the field-dependent masses with the thermal masses [7]:

$$m_i^2 \longrightarrow \mu_i^2(T) = \mu_i^2 + \Pi_i T^2, \quad (4.51)$$

where Π_i is the finite temperature mass function [6, 12], which can be calculated by taking the second derivative of Eq. (4.47) w.r.t. h, S and A. The relevant contributions for the considered model are listed in Appendix A.

In accordance with Refs. [6, 10, 12, 44], the counter term V_{ct} is included in the effective potential in order to maintain the minimization conditions stated in Eq. (4.32). It is as follows

$$V_{ct}(h, S, A) = \delta m_h^2 h^2 + \delta m_S^2 S^2, \tag{4.52}$$

where the relevant coefficients at zero temperature where $(h, S, A) = (v_h, v_S, 0)$, are given by

$$\begin{aligned} \delta m_h^2 &= \frac{1}{2v_h}\frac{\partial V_{CW}}{\partial h} \\ \delta m_S^2 &= \frac{1}{2v_S}\frac{\partial V_{CW}}{\partial S}. \end{aligned} \tag{4.53}$$

This ensures that the vevs of h and S, as well as the mass of A, will not be shifted. In order to compensate for the shift of the mass matrix of h and S, more complex terms would have to be added. However, since these shift are relatively small we do not include them here.

5 Constraints

When analyzing the $cxSM$ a number of factors related to DM collider and cosmological phenomenology, as well as constraints imposed by the requirement of GW generating FOEWPTs, and the possibility of baryogenesis, are taken into consideration when limiting the range for which the parameters of the model will have to be varied. The domain of detection made available through the realization of facilities like LISA, BBO and DECIGO will be of focus in this thesis, as its contributions will be vital for the field of GW and DM research - whether it be through experimental verification or further limiting the viable BSM range by imposed constraints.

The tree level potential in Eq. (4.30) has six free parameters after applying the tadpole conditions the quartic couplings λ_h and λ_S associated with the self-coupling of the Higgs and complex singlet, respectively; the quartic interaction coefficient λ_{hS} which signifies the strength of the interaction between the SM Higgs and the complex singlet; the vev of the S field, v_s; and the parameters a_1 and b_1 which are a result of symmetry breaking of the theory and determines the mass of the DM component A through the relationship described by the expression for m_A^2 Eq. (4.36). The quantities μ_h^2 and μ_S^2 are given in terms of the other parameters of the model, as demonstrated in Eq. (4.33). Fixed parameters of the model include the Higgs vev $v = 246.22$ GeV and the Higgs mass $m_h = 125.09$ GeV [41].

When analyzing the $cxSM$ with the cosmoTransition package a total of five physical observables, m_{h_1}, m_{h_2}, $\cos\theta$, $\mathrm{Br}(h \to AA)$ and $h^2\Omega_A$, are used as input parameters. This allows one to define an equal amount of Lagrangian parameters in terms of the physical observables. The Lagrangian parameters of interest to the $cxSM$ are a_1 and b_1, whose magnitude define the DM mass, and the quartic coupling parameters λ_h, λ_S and λ_{hS}. With the requirement for a theory which yields a stable DM, the main constraints of interest

are sourced from experimental DM research in combination with astrophysical observables such as the DM relic density. Below follows a short introduction to these subjects along with the equations necessary for a full analysis of the scalar potential.

5.1 Dark Matter

DM can be categorized into two subgroups: CDM and hot dark matter (HDM). Their classification is related to their relativistic nature, rather than temperature, and is an indication of how far the DM particles are able to move before being slowed down due to cosmic expansion; also referred to as the free streaming length (FSL). Considering a number of factors, with one of them being the mass structure formation of the early Universe, as observed in the cosmic microwave background (CMB), CDM is thought to be the most suitable DM candidate.

There are several sub-classes of CDM, with plausible DM masses varying over a wide span, from "fuzzy DM" at 10^{-21} eV, to heavy WIMPs in the TeV range. The two most common classifications are Weakly Interacting Massive Particles (WIMPs) and axions, where the mass difference of the particles of respective model (with the mass of the WIMP is generally in the GeV range, and the axion mass in the sub eV range) requires slightly different detection methods. The detection technology is also highly dependent on the interaction between the DM particle and the particles of the SM.

The field of DM detection can be divided into three subgroups: direct detection, where scientists hope to observe low-energy recoils of the nuclei of highly reactive fluids as a result of DM interaction; indirect detection, which includes cosmological observables (gamma-ray and neutrino measurements in particular) due to DM self-annihilation and decay; and collider measurements, by which constraints on decays and Higgs couplings to DM may be specified. Of specific interest to the $\mathbb{Z}_2 xSM$, are the Higgs related constraints which concern the coupling strength to the Higgs field, and the possibility of DM particle creation in colliders through the Higgs portal, which we would observe as invisible decays. These constraints, in relation to the capacity and sensitivity of both existing and proposed future colliders, will be taken into consideration when evaluating the DM aspect of the $cxSM$. However, one also needs to consider constraints imposed by astrophysical observables and the relic density, and include data from direct detection facilities in order to ensure that the viable range of the proposed model agrees with experimental research.

There are two possible DM outcomes for the $cxSM$: (a) a single component scenario where explicit symmetry breaking causes the Goldstone boson of the theory to acquire mass and thereby becoming the pseudoscalar DM candidate A, and (b) in which the vev of the scalar field S is equal to zero, resulting in a two component DM scenario involving both A and S. This thesis will focus on case (a), with the prospect of a theory which yields stable DM. For more information on scenarios where $v_s = 0$, the reader is referred to Refs. [11, 13, 14]. Constraints applicable to the $\mathbb{Z}_2 xSM$ and a stable DM scenario where $v_s \neq 0$, are - with emphasis on Higgs related collider constraints - listed below.

5.2 $\mathbb{Z}_2 xSM$

As mentioned before, one of the attractive features of the considered scalar extension to the SM is the fact that the DM mass of the model is independent of ones choice of scalar potential. Previous work in Ref. [13] have implemented DM mass in the GeV range, but in this thesis a mass range of 0.01 eV - 10 keV will be used for the numerical analysis.

Higgs related physics have a central role when developing the colliders of the future, and measurements of the Higgs potential is a high priority goal, since its reconstruction would reveal important information regarding the electroweak symmetry breaking. The coupling between the particles of the SM and the Higgs are (at the time of writing) uniquely determined in terms of the Fermi constant and the particles masses, but new physics BSM may modify these couplings in many ways. In order to identify a potential deviation from the SM, an essential aspect of Higgs related collider physics consists of measurements of the decay branching ratio times the Higgs production cross section [13]:

$$\xi^2 \equiv Br(\rightarrow invisible) \times \frac{\sigma_{BSM}}{\sigma_{SM}}. \tag{5.54}$$

The invisible decay branching fraction, $Br(h' \rightarrow invisible)$, associated with the $\mathbb{Z}_2 xSM$ is defined as $Br(h', S' \rightarrow AA)$, but since we do not have any information about the decay of the scalar S, this expression simplifies to

$$Br(h' \rightarrow AA) = \frac{\Gamma(h' \rightarrow AA)}{\Gamma(h' \rightarrow AA) + \Gamma(h' \rightarrow SM)}, \tag{5.55}$$

where $\Gamma(h' \rightarrow SM) = 4.07$ MeV [42] signifies the width of the coupling between the Higgs and the SM, and $\Gamma(h' \rightarrow AA)$ is given in Eq. (5.61). Relevant processes contributing to the decay widths can be seen below in Fig (2).

A vital aspect when analyzing the $\mathbb{Z}_2 xSM$, is to establish its contribution to the DM relic density Ω_{DM}, requiring that it does not exceed [32]

$$h^2 \Omega_{DM} = 0.102 \pm 0.010, \tag{5.56}$$

however, under-saturation is allowed since it permits the existence of DM other than the $\mathbb{Z}_2 xSM$. The DM relic density of the Universe is determined from acoustic peaks in the CMB, and there are two different scenarios in the early Universe, in which the DM relic density became relatively fixed; *freeze-out* and *freeze-in.*

1. Freeze-out

According to this scenario, the DM particles are in thermal equilibrium at high temperatures, but as the plasma temperatures drop below the mass of the DM, the Hubble expansion rate overpowers the processes responsible for the equilibrium, thus resulting in

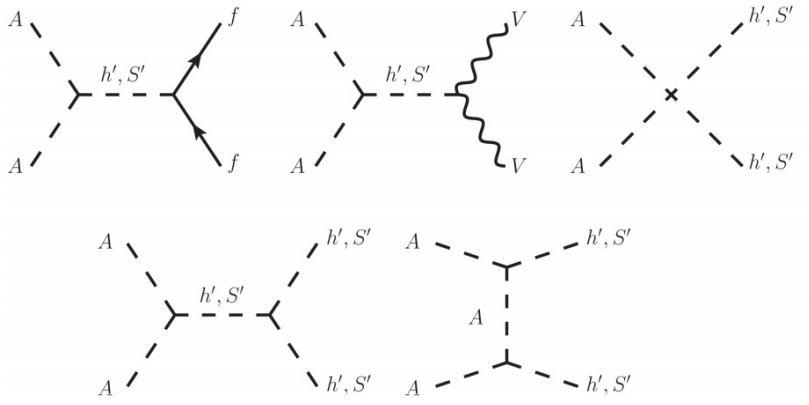

Figure (2) Feynman diagrams depicting the possible decay modes which contribute to the annihilation cross section of the DM particle A, with f and V being the fermions and the vector bosons of the SM, respectively. Image credit Ref. [13].

ceased interaction amongst particles; a freeze-out. In this model the comoving DM number density becomes fixed, and it is in general only dependent on the masses and couplings of the DM of the theory. This makes it an attractive scenario, since the necessary parameters may be independently measured in particle physics facilities, and therefore it is not dependent on the relatively unknown early thermal history of the Universe [43]. In a freeze-out scenario the relic density can be approximated as [44]

$$h^2\Omega_A = \frac{78}{g_*}\frac{m_A}{\text{keV}}, \tag{5.57}$$

where $g_* = 106.75$ is the number of relativistic d.o.f's at the electroweak scale. Applying the criteria that $h^2\Omega_A \simeq h^2\Omega_{DM}$, the DM mass can be constrained to the following range

$$0.112\text{keV} \leq m_A \leq 0.167\text{keV}. \tag{5.58}$$

2. Freeze-in

In the freeze-in process the DM is produced by the decay or annihilation of a heavier particle X, and therefore the DM relic density is directly proportional to the annihilation cross-section of the DM. For the $cxSM$, X represents the SM particles and since A only interacts with the SM via the Higgs, the relic density generally depends on the magnitude of the Higgs portal in Eq. (5.62). For the freeze-in scenario the relic density may be approximated as

$$h^2\Omega_A \simeq 2\frac{1.09\cdot 10^{27}}{g_*^{3/2}}\frac{m_A\Gamma(h'\to AA)}{m_h^2}, \tag{5.59}$$

where

$$\Gamma(h'\to AA) = \frac{1}{4\pi}\frac{\lambda_{hAA}^2}{m_h}\sqrt{1-4\frac{m_A^2}{m_h^2}}, \tag{5.60}$$

and λ_{hAA} is the effective Higgs-DM coupling, which in the mass eigenbasis is

$$\lambda_{hAA} = \frac{\lambda_{hS} v_h \cos\theta}{2}. \tag{5.61}$$

A small value for the portal coupling, $\lambda_{hS} \lesssim \mathcal{O}(0.01)$, is required in order to comply with experimental data. One of the main collider constraints of interest to the $\mathbb{Z}_2 xSM$, is the upper limit on the Higgs coupling to the DM, in our case to A, which determines the detectability of the pseudoscalar through the interaction with the SM Higgs. The prospects for finding evidence for a scalar model like the $cxSM$, when considering the DM of the theory, are limited in regards to colliders since the pair production of A via the Higgs means it could only observed indirectly through invisible decays and missing collision energy. To this date no invisible decays have been observed, but data from CMS [45] presents an upper bound on the Higgs invisible decay branching ratio of 0.15.

By solving Eq. (5.56) for $\Gamma(h', S \to AA)$ and combining the result with Eq. (5.60), one obtains an expression for the mass of the DM, whose form is convenient for the numerical analysis:

$$m_A = m_h^2 \frac{h^2 \Omega_A}{\kappa} \frac{[1 - Br(h' \to AA)]}{Br(h' \to AA)\Gamma(h' \to SM)} \quad \text{with} \quad \kappa \equiv 2\frac{1.09 \cdot 10^{27}}{g_*^{3/2}}. \tag{5.62}$$

In order to extract the parameters λ_h and λ_S, Eq. (4.39) is utilized in combination with the mass eigenvalues given in Eq. (4.34). λ_{hS} is found by combining Eqs. (5.61) and (5.62) by eliminating the parameter λ_{hAA}. This finally allows us to represent the Lagrangian parameters in terms of physical observables in the following manner

$$\begin{aligned} \lambda_h &= 2\frac{m_h^2 v_S - \sqrt{2} a_1}{v_S v_h^2} \\ \lambda_S &= \frac{2m_s^2}{v_S^2} \\ \lambda_{hS} &= \frac{m_h}{v_h \cos\theta} \sqrt{\frac{8\pi \mathrm{Br}(h' \to AA)}{\sqrt{1 - 4\frac{m_S^2}{m_h^2}}}}. \end{aligned} \tag{5.63}$$

6 Numerical analysis and discussion of results

As can be seen in Eq. (4.36), the mass of the DM of the $cxSM$ will depend on the linear coefficient a_1 and the quadratic coefficient b_1. Previous work has been presented in Ref. [13], where a fixed low value for $a_1 = 10^{-3}$ GeV^3 gives $m_A^2 \simeq b_1$. However, in this analysis both a_1 and b_1 will be treated as free parameters, and a_1 will be varied between 10^{-20} GeV^3 - 10^{-8} GeV^3, which - through the relation a_1/v_S will correspond to a mass range for

the $\mathbb{Z}_2 xSM$ of 0.01 eV - 10 keV, while b_1 will be given in terms of other parameters of the model by combining Eqs. (4.36) and (5.62) into the following expression

$$b_1 = \Big[m_h^2 \frac{h^2 \Omega_A}{\kappa} \frac{[1 - Br(h' \to AA)]}{Br(h' \to AA)\Gamma(h' \to SM)}\Big]^2 - \frac{\sqrt{2}a_1}{v_S}. \tag{6.64}$$

For the vev of the scalar field S, v_S, input values in the range 10 - 10^3 GeV^2 where chosen, and the mixing angle θ was varied between 0.01 - 0.15.

For the initial run with cosmoTransitions the mass range for the scalar S where set to $60\,\text{GeV} < m_S < 500\,\text{GeV}$, but since measuring points close to the sensitivity curves of LISA, BBO and DECIGO corresponded to the lower values of m_S, another run with $60\,\text{GeV} < m_S < 150\,\text{GeV}$ was initialized. The data from both results were combined and are presented below in Figs. 3-8. As can be seen in Figs. 3-7, there is one data point that is relatively close to the sensitivity curves of LISA, BBO, and DECIGO. For a better probability of detecting GWs, one should fine tune the input parameters of the model in order to examine this area in greater detail, with the hope of acquiring data points within the sensitivity range of detection. While there are relatively few and scarce data points close to the detection range, the majority of data points are represented by a peak frequency, f_{peak} of approximately $1 < 10^3$ Hz, and a corresponding value for the GW peak signal of $10^{-34} < h^2\Omega_{GW}^{peak} < 10^{-27}$.

The area representing the best range of detection roughly corresponds to a model with a mass eigenstate of $m_S = m_{h_2} \sim 150$ GeV (see Fig. 3a), and a mass eigenstate for the dark matter candidate of $\log_{10} m_A \sim -6$ eV, which corresponds to $m_A = 10^{-6}$ eV (see Fig 3b). In regards to the values for the vev, v_S, which can be seen in Fig 4a, detectable scenarios appears to be in the range of $v_S \simeq 100$ GeV, i.e. close to the scale at which electroweak symmetry takes place. As may be observed in Fig. 4b, the data points closest to the detection range correspond to a value of $\cos\theta$ close to 1. This translates to a value for θ close to zero, indicating that there is very little mixing amongst the mixing eigenstates h and S in the mass eigenstates h' and S', as can be seen in Eq. (4.41), i.e. $h' \simeq h$ and $S' \simeq S$

The relation $\Delta v_n/T_n$ for the two vevs of the $cxSM$, v_S and v_A, which may be seen in the plots in Fig. 5, show a similar scenario where the majority of data points depicts $v_{S,A} \sim 0$, i.e., the vevs hardly change over the course of the PT, and therefore contribute little to the over all energy budget of the PT. However, the points of interest which are close to the detection range indicate another scenario where $v_S > 1$, and $v_A > 5$, and suggests towards a scenario where there the initial and final value of the vevs are not equal, thus contributing to the energy budget of the PT. Fig. 6, which depicts the change of the Higgs vev in relation to the nucleation temperature, indicate that the change of v_h during the course of the PT for the scenarios closest to the detection domain, is close to zero. Even when considering the areas in the plot which is experiencing the largest change of the vev (corresponding to a peak frequency value of ~ 100 Hz), these values are considerably smaller than the maximum change of v_S and v_A. These results seems to indicate that v_h is

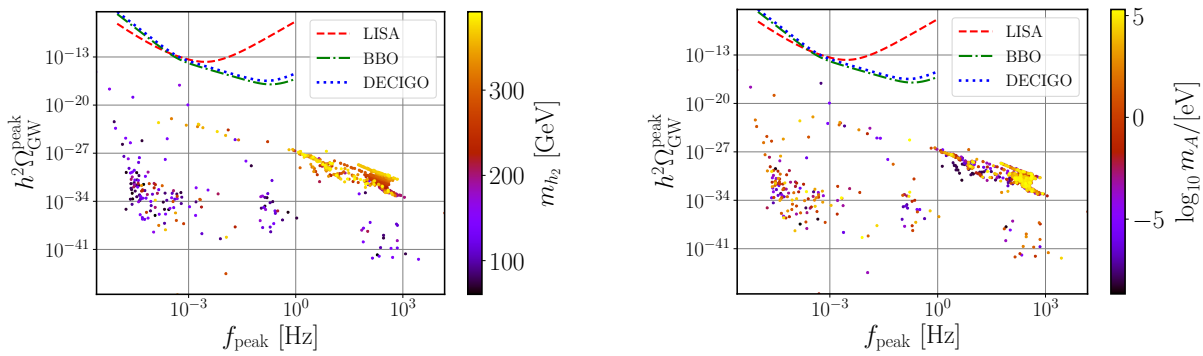

((a)) ((b))

Figure (3) Plot (a) is depicting the values for the mass eigenstate m_{h_2} and plot (b) is depicting the values for the mass eigenstate the dark matter candidate, m_A, of the $cxSM$. Both eigenstates are plotted against the net produced GW signal, $h^2\Omega_{GW}^{peak}$, and the peak frequency, f_{peak}. The value of each data point is indicated by the colour scheme, which is given to the right of the graph. The sensitivity range for LISA, BBO, DECIGO are indicated by the coloured lines.

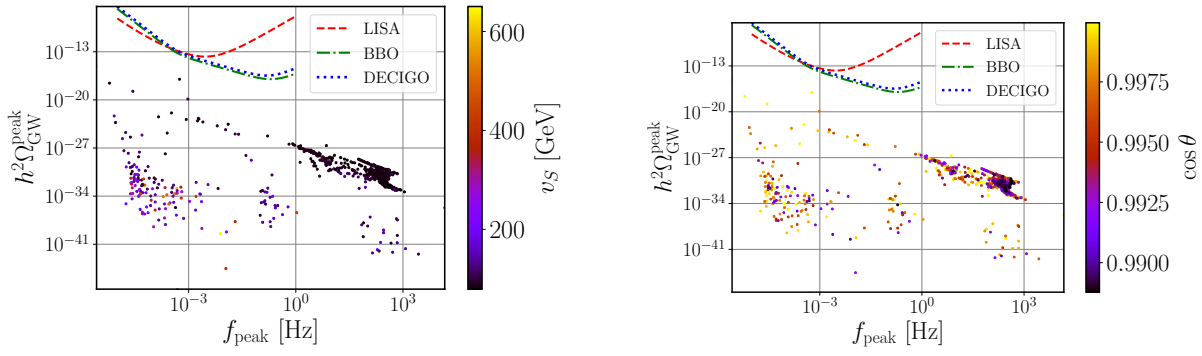

((a)) ((b))

Figure (4) Plot (a) is depicting the vev, v_S of the real component of the scalar field $\mathbb{S}$, and plot (b) is depicting the values for $\cos\theta$. Both v_S and $\cos\theta$ are plotted against the net produced GW signal, $h^2\Omega_{GW}^{peak}$, and the peak frequency, f_{peak}. The value of each data point is indicated by the colour scheme, which is given to the right of the graph. The sensitivity range for LISA, BBO, DECIGO are indicated by the coloured lines.

an overall more stable point than v_S and v_A. In addition to this one may conclude that v_h experience a larger change in magnitude for a larger value of the peak frequency, whereas the largest change in magnitude of v_S and v_A correspond to a lower peak frequency of $f_{peak} < 10^{-3}$ Hz and a rather high GW signal of $h^2\Omega_{GW}^{peak} > 10^{-20}$.

Fig. 7 depicts the GW parameters α and β/H, highest probability of detection is $\log_{10}\alpha > -2$ and $2 < \log_{10}\beta/H < 4$. In Fig. 8a. the nucleation temperature T_n is plotted as a function $\log_{10}\alpha$, and as can be seen, there are two areas with a nucleation temperature of

~ 25 and ~ 90, corresponding to a value of $\log_{10}\alpha \sim -6$ and $\log_{10}\alpha \sim -4$ respectively. For 8b. were T_n is plotted as function of β/H, there is a relatively scarce distribution of data points with small clusters of points where $T_n \sim 90$ and $T_n \sim 25$ corresponding to $\beta/H \sim 6$ and $\beta/H \sim 1$ respectively.

There are no plots for the SNR included in this result section, this is because there are no data points within the sensitivity range of either LISA, BBO or DECIGO. It should be mentioned that in order to produce more reliable and better results, the cosmoTransition package should be set to run for an extensive amount of time (preferably in the span of several weeks), in order to provide a larger amount of data points. The measuring points used for this analysis were collected after a total run of 5 days.

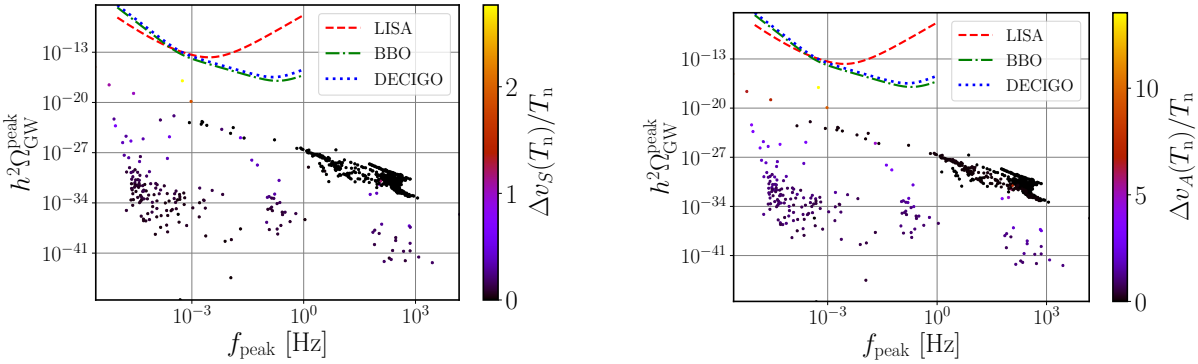

((a)) ((b))

Figure (5) Plot depicting the relation between the vevs of the complex scalar field, $\mathbb{S}$, at nucleation temperature, $v_{S,A}(T_n)$, and the nucleation temperature, T_n. Plot (a) shows the relation $\Delta v_S(T_n)/T_n$, and plot (b) depicts $\Delta v_A(T_n)/T_n$. Both relations in (a) and (b) are plotted against the net produced GW signal, $h^2\Omega_{GW}^{peak}$, and the peak frequency, f_{peak}. The value of each data point is indicated by the colour scheme, which is given to the right of the graph. The sensitivity range for LISA, BBO, DECIGO are indicated by the coloured lines.

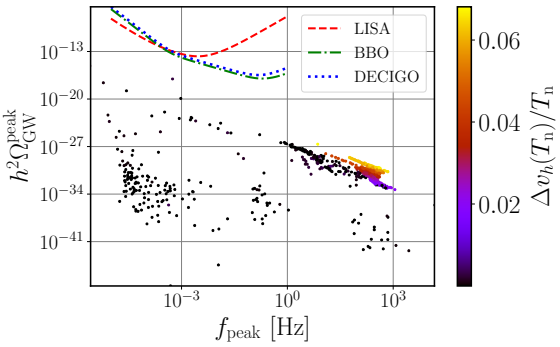

Figure (6) Plot depicting the relation between the Higgs vev at nucleation temperature, $v_h(T_n)$, and the nucleation temperature, T_n, as $\Delta v_h(T_n)/T_n$. Data points are plotted against the peak value of the corresponding net produced GW signal, $h^2\Omega_{GW}^{peak}$, and its peak frequency, f_{peak}. The sensitivity range for LISA, BBO, DECIGO are indicated by the coloured lines.

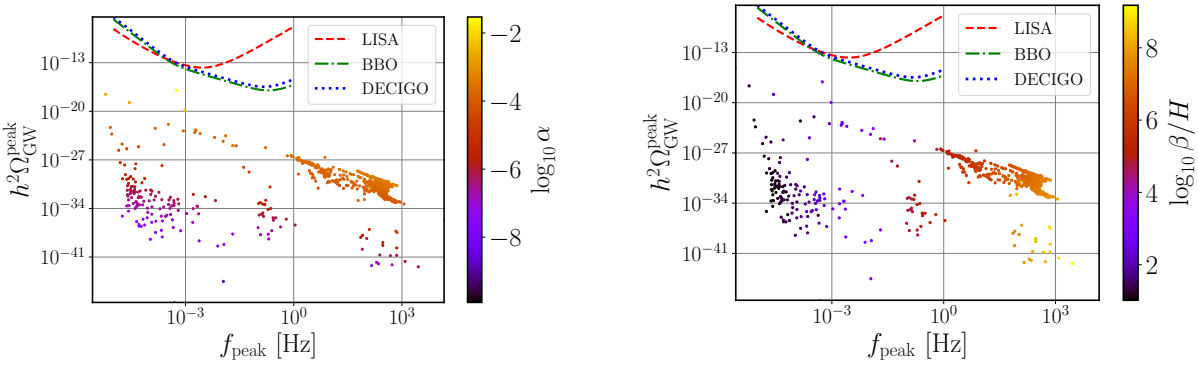

((a)) ((b))

Figure (7) The GW power spectra parameters α, (a), and β/H, (b), plotted against the peak value of the corresponding net produced GW signal, $h^2\Omega_{GW}^{peak}$, and its peak frequency, f_{peak}. The value of each data point is indicated by the colour scheme, which is given to the right of the graph. The sensitivity range for LISA, BBO, DECIGO are indicated by the coloured lines.

7 Conclusion

The advancement within the field of GW phenomenology has provided an additional window of physics, through which we are able to perceive and explore new areas and periods of the Universe, previously beyond our reach. In order to probe deeper into the fabric of cosmos and refine existing theoretical framework, the development of low frequency laser interferometry will play a crucial role by providing valuable constraints on the theoretical models. A direct detection of PGW's by facilities like LISA, BBO and DECIGO would suggest towards a model exhibiting electroweak first order phase transitions, such as the

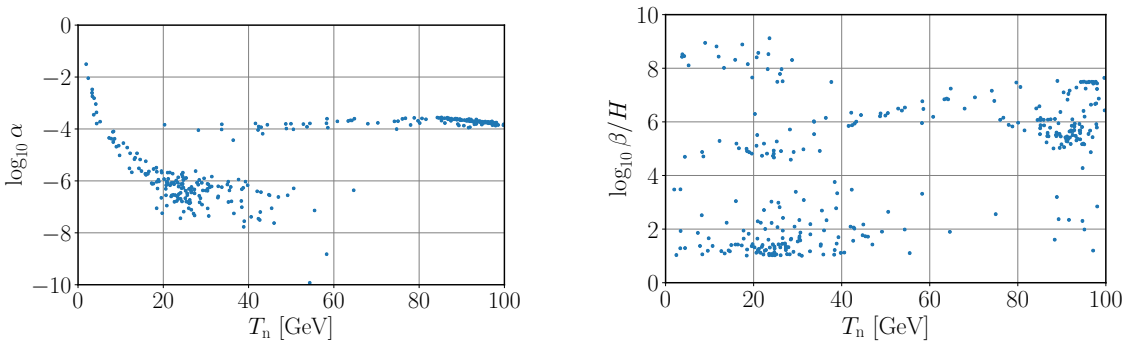

((a)) ((b))

Figure (8) Plots depicting the nucleation temperature, T_n, as a function of the GW power spectra parameters α, (a), and β/H, (b).

one examined throughout this thesis (although other model which exhibits FOEWPTs are not to be ruled out). Thus, progress in GW research will not only shed light on the dynamics of the early Universe, but evidently also play an important role in extending the framework of the SM, both w.r.t. a particle physics model which may include the force of gravity, but also in regards to dark matter phenomenology in terms of constraints and/or detection through GW experiments.

The LISA, BBO and DECIGO mission details may change over the coming years, which effects predictions of detectability of a given model, but providing that the sensitivity ranges remains approximately unchanged, there seems to be a good probability of PGW detection. For the condition examined in this thesis, the best probability of detection appears to be for a dark matter scalar with a mass around 50 GeV. A more extensive analysis could be done by varying the input parameter a_1 over a larger span, which would result in a slightly different mass range for the dark matter of the model. The mass of the scalar S could also be limited as to further increase the probability of a GW peak signal closer to LISA, BBO and DECIGO.

Appendices

A Thermal corrections

The number of d.o.f. for the particles who contribute to the thermal correction, $V_{th}(h, S, A, T)$, and the effective potential, are as follows

$$n_W = 6, \qquad n_Z = 3, \qquad n_\gamma = 2, \tag{A.65}$$

where γ is the transversely polarized photon. For the longitudinal polarized photon

$$n_s = 6, \qquad n_{A_L} = 1, \tag{A.66}$$

and for the fermionic contributions

$$n_{u,d,c,s,t,b} = 12, \qquad n_{e,\mu,\tau}, \qquad n_{\nu_{1,2,3}} = 2. \tag{A.67}$$

The finite temperature mass functions Π_i are given by

$$\begin{aligned}
\Pi_h &= \frac{3}{16}g_L^2 + \frac{1}{16}g_Y^2 + \frac{1}{8}\lambda_h + \frac{1}{24}\lambda_{hS} + \frac{1}{4}(y_t^2 + y_b^2 + y_c^2 + y_s^2 + y_u^2 + y_d^2) + \frac{1}{12}(y_\tau^2 + y_\mu^2 + y_e^2), \\
\Pi_S &= \Pi_A = \frac{1}{12}(\lambda_S + \lambda_{hS}).
\end{aligned} \tag{A.68}$$

The thermal corrections to the gauge sector of the SM is

$$M^2_{gauge}(h,T) = M^2_{gauge}(h) + \frac{11}{6}T^2 \begin{pmatrix} g^2 & 0 & 0 & 0 \\ 0 & g^2 & 0 & 0 \\ 0 & 0 & g^2 & 0 \\ 0 & 0 & 0 & g^2 \end{pmatrix}, \tag{A.69}$$

where the eigenvalues for the zero-temperature mass matrix M^2_{gauge} are given by

$$\begin{aligned}
m_W^2 &= \frac{1}{4}h^2 g_L^2 \\
m_Z^2 &= \frac{1}{4}h^2(g_L^2 + g_Y^2).
\end{aligned} \tag{A.70}$$

For the thermal masses, only the longitudinal polarizations of the gauge bosons; W_L^+, W_L^-, Z_L and A_L, acquire thermal corrections, while the mass of the transversely polarized photon, m_γ remains zero. These eigenvalues are as follows

$$\begin{aligned}
m^2_{W_L}(h,T) &= m_W^2(h) + \frac{11}{6}g^2T^2, \\
m^2_{Z_L,A_L}(h,T) &= \frac{1}{2}m_Z^2(h) + \frac{11}{12}(g_L^2 + g_Y^2)T^2 \pm \mathcal{D},
\end{aligned} \tag{A.71}$$

where the field-dependent masses for the W and Z bosons are given by Eq. (A.69), and $\mathcal{D}$ reads as follows

$$\mathcal{D}^2 = \Big(\frac{1}{2}m_Z^2(h) + \frac{11}{12}(g_L^2 + g_Y^2)T^2\Big)^2 - \frac{11}{12}g_L^2 g_Y^2 T^2\Big(h^2 + \frac{11}{3}T^2\Big). \tag{A.72}$$

B Efficiency Coefficients

The semi-analytical approach to the efficiency coefficients are given here in terms of the Chapman-Jouguet speed, v_J, and the bubble wall velocity, v_b. The fraction of vacuum energy that is converted to kinetic energy of the fluid is as follows,

$$\kappa = \frac{(v_J - 1)^3 v_J^{5/2} v_b^{-5/2} \kappa_1 \kappa_2}{\left[(v_J - 1)^3 - (v_b - 1)^3\right] v_J^{5/2} \kappa_1 + (v_b - 1)^3 \kappa_2} \tag{B.73}$$

where κ_1 denotes the efficiency factor in the limit of Jouguet detonations where $v_b = v_J$,

$$\kappa_1 = \frac{\sqrt{\alpha}}{0.135 + \sqrt{0.98 + \alpha}}, \tag{B.74}$$

κ_2 is the efficiency factor for large bubble wall velocities, i.e., $v_b \longrightarrow 1$,

$$\kappa_2 = \frac{\alpha}{0.73 + 0.083\sqrt{\alpha} + \alpha}, \tag{B.75}$$

and the Chapman-Jouguet speed is denoted by

$$v_J = \frac{1}{1 + \alpha}\left(c_s + \sqrt{\alpha^2 + \frac{2}{3}\alpha}\right). \tag{B.76}$$

References

[1] G. Aad, T. Abajyan, B. Abbott, et al., *Observation of a New Particle in the Search for the Standard Model Higgs Boson with the ATLAS Detector at the LHC*, (2012), arXiv: 1207.7214 [hep-ex].

[2] CMS Collaboration, *Watching the top quark mass run* [Online: accessed 04-05-2021] URL: https://cms.cern/news/watching-top-quark-mass-run.

[3] D. Clowe, M. Bradac, A. H. Gonzalez et al., *A Direct Empirical Proof of the Existence of Darm Matter*, (2006), arXiv: 0608407 [astro-ph].

[4] The Oskar Klein Centre, Department of Physics, Stockholm University. *Dark Matter Evidence, Particl Pysics Candidates and Detection Methods.* 2012. arXiv: 1205.4882 [astro-ph.HE].

[5] J. M. Cline and K. Kainulainen, *Electroweak baryogenesis and dark matter from a singlet Higgs*, (2013), arXiv: 1210.4196 [hep-ph].

[6] T. Vieua, A. P. Morais, and R. Pasechnik, *Electroweak phase transitions in multi-Higgs models: the case of Trinification-inspired THDSM* , (2018), arxiv: 1801.02670 [hep-ph].

[7] A. P. Morais and R. Pasechnik, *Probing multi-step electroweak phase transition with multi-peaked primordial gravitational waves spectra*, (2020), arXiv: 1910.00717 [hep-ph].

[8] G. C. Branco, P. M. Ferreira, L. Lavoura, et al., *Theory and phenomenology of two-Higgs-doublet models*, (2011), arXiv: 1106.0034 [hep-ph].

[9] J. M. Cline, K. Kainulainen, and M Trott, *Electroweak Baryogenesis in Two Higgs Doublet Models and B meson anomalies*, (2011), arXiv: 1107.3559 [hep-ph].

[10] L. Frommea, S. J. Huberb, and M. Seniucha, *Baryogenesis in the Two-Higgs Doublet Model*, (2006), arXiv: 0605242 [hep-ph].

[11] V. Barger, P. Langacker, M. McCaskey, et al., *Complex singlet extension of the Standard Model*, (2009), arXiv:0811.0393 [hep-ph].

[12] M. Jiang, L. Bian, W. Huang, and J. Shu, *Impact of a complex singlet: electroweak baryogenesis and dark matter*, (2016), arXiv: 1502.07574 [hep-ph].

[13] M. Gonderinger, H. Lim, and M. J. Ramsey-Musolf, *Complex Scalar Singlet Dark Matter: Vacuum Stability and Phenomenology*, (2012), arXiv: 1202.1316 [hep-ph].

[14] C. Chiang, M. J. Ramsey-Musolf, and E. Senaha, *Standard Model with a Complex Scalar Singlet: Cosmological Implications and Theoretical Considerations*, (2017), arXiv: 1707.09960 [hep-ph].

[15] R. Costa, A. P. Morais, M. O. P. Sampaio, and R. Santosa, *Two-loop stability of a complex singlet extended Standard Model*, (2015), arXiv: 1411.4048 [hep-ph].

[16] R. Coimbra, M. O. P. Sampaio, and R. Santos, *ScannerS: Constraining the phase diagram of a complex scalar singlet at the LHC*, (2013), arXiv: 1301.2599 [hep-ph].

[17] A. D. Sakharov, *Violation of CP invariance, C asymmetry, and baryon asymmetry of the Universe*, (1967), *Pisma Zh. Eksp. Teor. Fiz.* **5**, 32–35. [Usp. Fiz. Nauk161,61(1991)].

[18] N. Bernala and F. Hajkarim, *Primordial Gravitational Waves in Nonstandard Cosmologies*, (2019), arXiv: 1905.10410 [astro-ph.CO].

[19] Y. Cui, M. Lewicki, D. E. Morrissey, and J. D. Wells, *Cosmic Archaeology with Gravitational Waves from Cosmic Strings*, (2017), arXiv: 1711.03104 [hep-ph].

[20] A. Kormu, *Simulating Bubble Nucleation in the Electroweak Phase Transition*, (2020), Master's Thesis, University of Helsinki. [Online: accessed 08-05-2021] URL: https://helda.helsinki.fi/bitstream/handle/10138/318463/Kormu_Anna_masters_thesis_2020.pdf

[21] M. Hindmarsh, M. Lüben, J. Lumma, and M. Pauly, *Phase transitions in the early universe*, (2021), arXiv: 2008.09136 [astro-ph.CO].

[22] C. Wainwright, *CosmoTransitions: Computing Cosmological Phase Transition Temperatures and Bubble Profiles with Multiple Fields*, (2011), arXiv:1109.4189 [hep-ph].

[23] L. Leitao, A. Mégevand, and A. D. Wánchez, *Gravitational Waves from the electroweak Phase Transition*, (2012), arXiv: 1205.3070 [astro-ph.CO].

[24] C. Corianò, P. H. Frampton, and Alessandro Tatullo, *Conformal Unification in a Quiver Theory and Gravitational Waves*, (2020), arXiv: 2005.12216 [hep.ph].

[25] R. A. Battye and E. P. S Shellard, *Primordial Gravitational Waves: a probe of the early Universe*, (1996), arXiv: astro-ph/9604059v1.

[26] M. D'Onofrio and K. Rummukainen, *The Standard Model cross-over on the lattice*, (2015), arXiv: 1508.07161 [hep-ph].

[27] NASA, ESA, *LISA, Laser Interferometer Space Antenna*, [Online: accessed 08-05-2021], URL: https://lisa.nasa.gov.

[28] V. Corbin and N. J. Cornish, *Detecting the Cosmic Gravitational Wave Background with the Big Bang Observer*, (2005), arXiv: gr-qc/0512039

[29] S. Kawamura, M. Ando, N. Seto, et al., *Current status of space gravitational wave antenna DECIGO and BDECIGO*, (2020), arXiv: 2006.13545 [gr-qc].

[30] N. Karnesis, M. Lilley, A. Petiteau, *Assessing the detectability of a Stochastic Gravitational Wave Background with LISA, using an excess of power approach*, (2020), arXiv: 1906.09027 [astro-ph.IM].

[31] C. Caprinia, M. Chalab, and G. C. Dorsch, *Detecting gravitational waves from cosmological phase transitions with LISA: an update*, (2021), arXiv: 1910.13125 [astro-ph.CO].

[32] Planck Collaboration: N. Aghanim, Y. Akrami, M. Ashdown et al., *Planck 2018 results. VI. Cosmological parameters*, (2018), arXiv: 1807.06209 [astro-ph.CO].

[33] C. Corianò, P. H. Frampton, and A. Tatullo, *Conformal Unification in a Quiver Theory and Gravitational Waves*, (2020), arXiv: 2005.12216 [hep-ph].

[34] D. J. Weir, *Gravitational waves from a first-order electroweak phase transitio: a brief review*, (2018), arXiv: 1705.01783 [hep-ph].

[35] M. Hindmarsh, S. J. Huber, K. Rummukainen, and D. J. Weir, *Shape of the acoustic gravitational wave power spectrum from a first order phase transition*, (2020), arXiv: 1704.05871 [astro-ph.CO].

[36] J. R. Espinosa, T. Konstandin, J. M. Noc, and G. Servant, *Energy Budget of Cosmological First-order Phase Transitions*, (2010), arXiv: 1004.4187 [hep-ph].

[37] J. M. No, *Large gravitational wave background signals in electroweak baryogenesis scenarios*, (2011), arXiv: 1103.2159 [hep-ph].

[38] H. H. Patel and M. J. Ramsey-Musolf, *Baryon Washout, Electroweak Phase Transition, and Perturbation Theory*, (2015), arXiv: 1101.4665 [hep-ph].

[39] M. Hindmarsh and M. Hijazi, *Gravitational waves from first order cosmological phase transitions in the Sound Shell Model*, (2019), arXiv: 1909.10040 [astro-ph.CO].

[40] U. Pen and N Turok, *Shocks in the Early Universe*, (2016), arXiv: 1510.02985 [astro-ph.CO].

[41] The ATLAS and CMS Collaborations, *Combined Measurement of the Higgs Boson Mass in pp Collisions at $\sqrt{s}$ = 7 and 8 TeV with the ATLAS and CMS Experiments*, (2015), arXiv: 1503.07589 [hep-ex].

[42] CERN European Organization for Nuclear Research, *Handbook of LHC Higgs cross sections: 3. Higgs Properties, Report of the LHC Higgs Cross Section Working Group*, (2013), arXiv: 1307.1347 [hep-ph].

[43] F. D'Eramo, N. Fernandez, and S. Profumo, *Dark Matter Freeze-in Production in Fast-Expanding Universes*, (2018), arXiv: 1712.07453 [hep-ph].

[44] M. Frigerio, T. Hambye, and E. Masso, *Sub-GeV dark matter as pseudo-Goldstone from the seesaw scale*, (2011), arXiv: 1107.4564 [hep-ph].

[45] The CMS Collaboration, *Search for invisible decays of a Higgs boson produced through vector boson fusion in proton-proton collisions at* $\sqrt{s}$ *= 13 TeV*, (2019), arXiv: 1809.05937 [hep-ex].

[46] E. Thrane and J. D. Romano, *Sensitivity curves for searches for gravitational-wave backgrounds*, (2013), arXiv: 1310.5300v2 [astro-ph.IM].

[47] C. J. Moore, R. H. Cole, and C. P. L. Berry, *Gravitational-wave sensitivity curves*, (2014), arXiv: 1408.0740 [gr-qc].

[48] K. Nakayama and J. Yokoyama, *Gravitational Wave Background and Non-Gaussianity as a Probe of the Curvaton Scenario*, (2009), arXiv: 0910.0715 [astro-ph.CO].